https://doi.org/10.1070/QEL16766

Parametric generation in a PPLN crystal pumped by a *Q*-switched mode-locked Nd:YAG laser: comparison of the superluminescent and singly resonant operation regimes

V.I. Donin, D.V. Yakovin, A.V. Gribanov, M.D. Yakovin

Abstract. **The output characteristics of light in two parametric generation regimes [parametric superluminescence and parametric generation in a singly resonant optical parametric oscillator (OPO) based on a 50-mm long PPLN crystal, synchronously pumped by a 50-ps Nd:YAG laser] are compared. The total average output power at the wavelengths of signal (λ = 1475 nm) and idler (λ = 3820 nm) waves in the superluminescence regime is ~120 mW (peak power ~120 kW). The maximum total conversion efficiency with respect to the absorbed power in the superluminescence regime is ~60%. The maximum conversion efficiency into the idler wave with respect to the absorbed pump power is 15% and 25% (quantum efficiencies of 54% and 90%) for the superluminescence and singly resonant OPO regimes, respectively. The maximum values of the average output power at the idler wavelength are ~30 and ~60 mW at degrees of pump depletion of 47% and 55% for the superluminescence and singly resonant OPO regimes, respectively.**

Keywords: *optical parametric oscillator, mid-IR range, synchronous pumping, parametric superluminescence.*

1. Introduction

Periodically poled lithium niobate (PPLN) crystals pumped by picosecond lasers with a high peak power may provide efficient parametric generation in different regimes, both using a cavity (see, e.g., [1, 2]) and without it (superluminescent generation) [3–6]. Previously [6], we demonstrated efficient superluminescent parametric generation with the highest (as compared with the published data) conversion efficiency (above 80% of absorbed pump power) under pumping by a *Q*-switched mode-locked (QML) Nd:YAG laser. The ways to improve the output characteristics using a cavity were not considered in [6]. At the same time, there are only few publications considering the influence of cavity on the characteristics of parametric generation with high amplification in a PPLN crystal under picosecond pumping, and the published results are not quite clear. For example, the characteristics of parametric generation in the cavity-free and cavity regimes under pumping by a disk passively mode-locked Yb:YAG laser were compared in [4], whereas a *Q*-switched Nd:YLF laser was used as a pump source in [7]. An increase in the idler wave power by ~10% in the cavity regime in comparison with the cavity-free conditions at a pump intensity of ~0.2 GW cm^{-2} was observed in [4, 7]. The pump intensity used in [2] was ~2 GW cm^{-2}, and the aforementioned power increased by a factor of ~3; however, the working crystal length was smaller by a factor of 2.5 than that used in [6]. In this paper, we report experimental results and compare the output characteristics of parametric generation in the superluminescence and singly resonant generation regimes implemented in a 50-mm-lomg PPLN crystal pumped by a 50-ps QML Nd:YAG laser.

V.I. Donin, D.V. Yakovin, A.V. Gribanov, M.D. Yakovin Institute of Automation and Electrometry, Siberian Branch, Russian Academy of Sciences, prosp. Akad. Koptyuga 1, 630090 Novosibirsk, Russia; e-mail: donin@iae.nsk.su

Received 27 June 2018; revision received 27 July 2018
Kvantovaya Elektronika **48** (10) 936–940 (2018)
Translated by Yu.P. Sin'kov

2. Parametric superluminescence

A schematic of the cavity-free optical parametric generator (OPG) used in this study is shown in Fig. 1; it is similar to that described in [6].

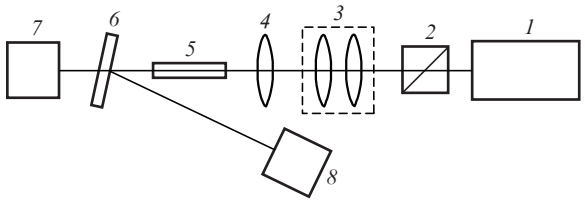

Figure 1. Schematic of the experimental observation of the superluminescence regime: (*1*) QML Nd:YAG laser; (*2*) polarisation power controller; (*3*) objective; (*4*) focusing lens; (*5*) nonlinear PPLN crystal; (*6*) filter; (*7*, *8*) power meters.

The QML Nd:YAG laser described in [8, 9] was used as a pump source. Its linearly polarised radiation is a set of pulse trains ~150 ns long with a repetition rate of 2 kHz; individual pulses in a train had a width of ~50 ps and a repetition rate of 100 MHz. The maximum average and peak powers were ~400 mW and ~0.15 MW, respectively. The laser beam was focused in a nonlinear PPLN crystal by lens (*4*) with a focal length of 280 mm. The pump beam waist in the crystal was 160 μm in diameter. The pump power was controlled by polarisation controller (*2*). Objective (*3*) was applied to reduce the pump beam divergence by a factor of 3.5. The total beam divergence after the objective was ~0.57 mrad. Filter (*6*) was either a mirror with a high reflectance at λ = 1064 nm or a germanium plate when measuring the total or idler power, respectively. The idler and total powers were measured by power meter (*7*) (OPHIR), and the pump power transmitted through the crystal was measured by power meter (*8*) (Gentec). The PPLN crystal doped with MgO (5 mol %)

was $5 \times 1 \times 50$ mm in size and had a period of regular domain structure $\Lambda = 29.5$ μm. Antireflection coatings with reflectances $R < 1\%$ at $\lambda = 1.064$ μm, $R < 2\%$ at $\lambda = 1.4–1.5$ μm, and $R < 1\%$ at $\lambda = 3.6–3.8$ μm were deposited on the crystal end faces. All measurements were performed at a crystal temperature of 24 °C.

Figure 2 shows dependences of the output power of signal ($\lambda = 1475$ nm) and idler ($\lambda = 3820$ nm) waves on the pump power, which were obtained in the superluminescence regime.

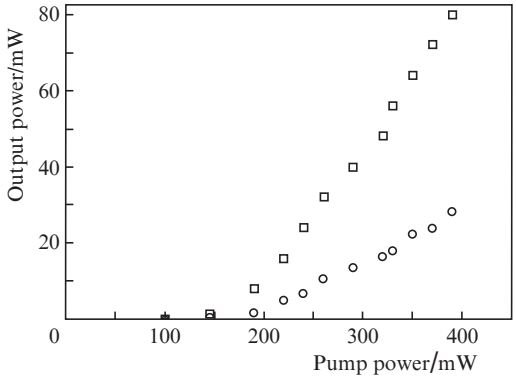

Figure 2. Dependences of the output power of the (□) signal and (○) idler waves on the pump power in the superluminescence regime.

The maximum values of the average output power of the idler and signal waves were ~30 and ~80 mW at conversion efficiencies of ~7.2% and ~21%, respectively. The threshold pump power was 100 mW.

We also measured the pump power at the output of the PPLN crystal, P_{out}, as a function of its value at the crystal input, P_{in}; this dependence was used to calculate the pump depletion coefficient (Fig. 3):

$$\eta = 1 - \frac{P_{out}}{P_{in}}. \tag{1}$$

The maximum value of η was 47% ± 3%. Hence, the conversion efficiency with respect to the absorbed pump power was ~60% and ~15% for the total and idler waves, respectively.

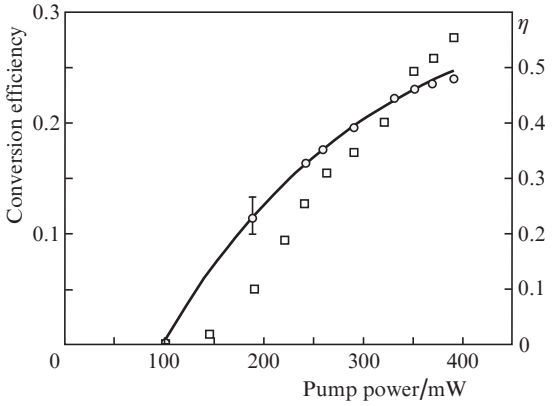

Figure 3. Dependences of the (□) total conversion efficiency and (○) pump depletion coefficient on the pump power in the superluminescence regime. The solid curve is an approximation.

The pump depletion coefficient for a double pass through a nonlinear crystal was measured applying the scheme presented in Fig. 4. Spherical copper mirror (*6*) was installed at a distance H from the pump beam waist in the PPLN crystal; this distance was chosen so as to make the mirror curvature radius ($r = 125$ mm) almost coincide with the wavefront curvature radius; i.e., $H \approx r$. Sapphire plate (*9*) was used to reflect some part of pump radiation to a power meter after the double pass of the pump beam through the nonlinear crystal. The depletion coefficient was calculated from the formula

$$\eta = 1 - \frac{P_{out}}{R[(1-R)P_{in}]}, \tag{2}$$

where R is the reflectance from two plate faces, P_{out} is the pump power arriving at the power meter, and P_{in} is the pump power before the sapphire plate. At $P_{in} = 360$ mW, the coefficient η for two passes was 50%, whereas for one pass the η value was 45%.

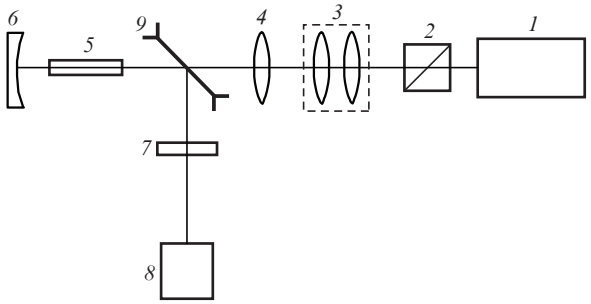

Figure 4. Schematic for measuring the pump depletion coefficient for two passes: (*1*) QML Nd:YAG laser; (*2*) pump power controller; (*3*) objective; (*4*) focusing lens; (*5*) nonlinear PPLN crystal; (*6*) copper spherical mirror; (*7*) narrow-band filter at $\lambda = 1064$ nm; (*8*) power meter; (*9*) sapphire plate.

The beam divergence in the superluminescence regime is determined by the emitting region geometry, i.e., in fact, by the divergence of the pump wave incident on the crystal [6]. The superluminescence divergence in the far-field zone (at a distance of 2 m from the PPLN crystal), measured in the horizontal plane at $\lambda = 619$ nm (the sum of signal and pump waves), amounted to 33 ± 5 mrad. The measurements were performed according to the scheme presented in Fig. 1: the radiation reflected from filter (*6*) passed through a light filter KS-15 to arrive at photodetector (*8*) (FD-2 photodiode with a sensitive-area diameter of 1.3 mm), which was mounted on a translation stage and moved in the horizontal direction perpendicular to the laser beam axis. The same divergence was obtained for the signal and idler waves. These data coincided (within the measurement error) with the results of [6]. The threshold pump power of 100 mW corresponds to the power density in the waist: ~200 MW cm^{-2}. The value of this power density was calculated from the formula [10]

$$I_{th} = 5\frac{\varepsilon_0 c \lambda_s \lambda_i}{FL^2} \tag{3}$$

to be 160 MW cm^{-2}, which is in good agreement with the measurement results. In formula (3), $\varepsilon_0 = 8.85 \times 10^{-14}$ F cm^{-1} is the dielectric constant; $\lambda_s = 1475$ nm and $\lambda_i = 3820$ nm are, respec-

tively, the wavelengths of signal and idler waves; $F = d_{\text{eff}}^2/n^3 = 19.75$ pm^2 V^{-2} is the nonlinear optical quality factor of the crystal; d_{eff} is the effective nonlinearity coefficient; n is the refractive index of the nonlinear crystal; and $L = 5$ cm is the nonlinear crystal length.

The found total conversion efficiency with respect to the absorbed power (~60%) is below the value obtained by us in [6]. This is apparently related to the lower quality of the crystal in use (as confirmed by a higher generation threshold).

3. Singly resonant OPO regime

A schematic of a singly resonant synchronously pumped OPO is presented in Fig. 5; it is similar to that used in [2]. The difference is as follows: in this study, the PPLN crystal length was 50 mm (20 mm in [2]) and the focal length of the focusing lens was 280 mm (250 mm in [2]). Pumping was performed by the above-described QML Nd : YAG laser with a pulse train repetition rate of 2 kHz. The OPO cavity was formed by mirrors (*7–9*). Mirror (*7*) had a curvature radius of 100 mm, a reflectance $R_{1.4-1.7} = 99.5\%$ at $\lambda = 1.4-1.7$ μm, and a transmittance of about 99% at $\lambda = 1.064$ μm. Copper mirror (*8*) had a curvature radius of 125 mm and a reflectance $R_{1.0-1.7} = 90\%$ and $R_{3.0-4.0} = 97\%$. Flat output mirror (*9*) on a ZnSe substrate ($R_{1.2-1.7} = 99.5\%$) had a transmittance of 78% at $\lambda = 1.06$ μm and 99.5% at $\lambda = 3.0-4.0$ μm. This mirror could be moved along the cavity axis using an adjusting device.

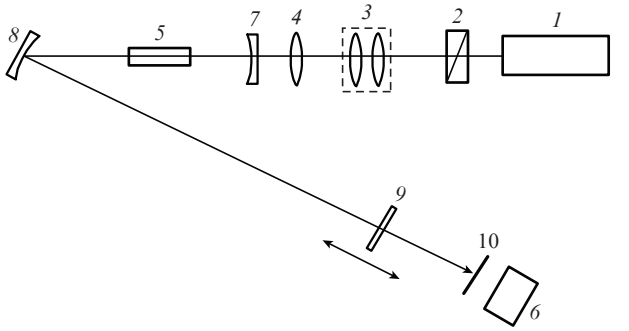

Figure 5. Schematic of a singly resonant OPO: (*1*) QML Nd : YAG laser; (*2*) power controller; (*3*) objective; (*4*) focusing lens; (*5*) nonlinear PPLN crystal; (*6*) power meter (OPHIR); (*7–9*) OPO cavity mirrors; (*10*) germanium plate.

The OPO generation threshold was 60 mW, which corresponds to $I_{\text{th}} = 120$ MW cm^{-2}. This value differs significantly from that calculated using the formula from [11, 12]:

$$I_{\text{th}} = \frac{l}{L^2}\frac{n^3\varepsilon_0 c\lambda_s\lambda_i}{8\pi^2 d_{\text{eff}}^2 g_s g_t h_{\text{sm}}} \approx 13 \text{ MW cm}^{-2}, \quad (4)$$

where $l = 0.3$ is the total loss in the cavity for a double pass at the signal wavelength, $g_s = 0.4$ is the spatial matching coefficient, $g_t = 0.6$ is the temporal matching coefficient, and $h_{\text{sm}} = 0.1$ (the function h_{sm} was defined in [11]). Apparently, this difference is due to the fact that we determined the generation threshold visually (through a red light filter), from the instant of occurrence of radiation with $\lambda = 619$ nm on the cavity mirror, i.e., in fact, the occurrence threshold for the radiation with the sum frequency $\omega_s + \omega_p$ (ω_s and ω_p are the signal and pump frequencies, respectively) was observed.

At the maximum pump power, the average output power of the idler wave ($\lambda = 3820$ nm) was ~60 mW.

We also measured the pump power transmitted through the OPO cavity in the absence of a nonlinear crystal. Based on the measurement results, the dependence of the pump depletion coefficient on the pump power was calculated from the formula

$$\eta_{\text{res}} = 1 - (1+\alpha)\frac{P_{\text{out}}}{P_{\text{in}}}, \quad (5)$$

where $\alpha = 0.28$ is the absorption loss (measured at $\lambda = 1064$ nm) in the cavity mirrors, P_{in} is the pump power incident on the crystal, P_{out} is the measured pump power transmitted through the cavity with nonlinear crystal, and $(1+\alpha)P_{\text{out}}$ is the calculated pump power at the output of the nonlinear crystal in the cavity. Dependence (5) is presented in Fig. 6.

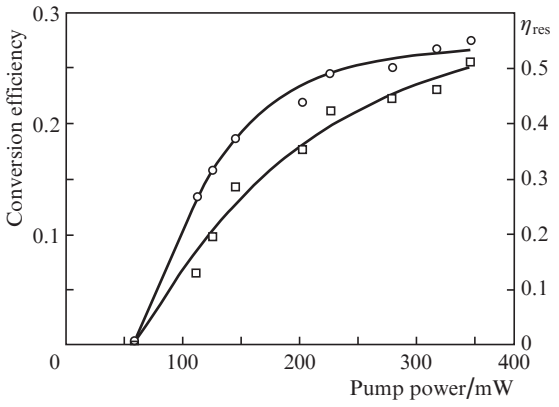

Figure 6. Dependences of the (□) conversion efficiency into the idler wave with respect to the absorbed power and (○) the pump depletion coefficient in the OPO cavity on the pump power incident on the crystal. The solid curves are approximations.

The maximum value of the depletion coefficient was ~55% at a pump power of 360 mW, which exceeds the corresponding values in the superluminescence regime for one (45%) and two (50%) pump radiation passes through the PPLN crystal.

We also calculated the conversion efficiency into the idler wave with respect to the absorbed pump power. It can be seen in Fig. 6 that maximum conversion efficiency is ~25%, which corresponds to a quantum conversion efficiency of ~90%. Taking into account that the absorption coefficient in the working crystal at the idler wavelength (3820 nm) is ~19% [6], the quantum efficiency with respect to the absorbed power reaches ~110%.

The radiation divergence at the idler and signal wavelengths was measured in the far-field zone at a distance of 5 m. The OPO radiation was extracted from the cavity using a sapphire plate located near the flat output mirror. A germanium plate was applied to filter the radiation at the idler wavelength, and a plane mirror (dense for $\lambda = 1064$ nm) and an IKS-5 light filter were used to filter the radiation at the signal wavelength. The detector was installed on an $x-y$

stage, which could be moved along the horizontal (along the x axis in the cavity plane) and vertical (along the y axis perpendicular to the cavity plane) directions, perpendicular to the beam propagation. The spatial distribution of the beam intensity over the x and y axes was measured, and the values found were used to calculate the total beam divergence. The measurements at the signal and idler wavelengths were performed using, respectively, a germanium photodiode FD-2 and a pyrometer MG-30 (with a detection area of 1 mm^2). The photodetector data were recorded on a digital oscilloscope (see Fig. 7).

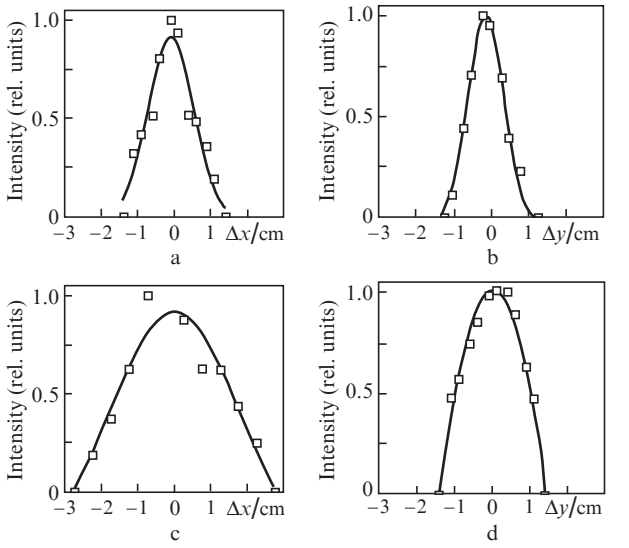

Figure 7. Spatial distributions of the radiation intensity over the (a, c) x and (b, d) y axes in the far-field zone at the (a, b) signal wavelength of 1475 nm and (c, d) idler wavelength of 3820 nm.

The total divergence of the output radiation, measured at the idler wavelength in the far-field zone along the x and y axes, was found to be $\Theta_x = 6$ mrad and $\Theta_y = 4$ mrad, respectively; the measurements at the signal wavelength yielded $\Theta_x = 3$ mrad and $\Theta_y = 2.6$ mrad. The difference in the divergences along the x and y axes is caused by the astigmatism of the pump laser cavity [13]. The error in measuring the divergences was ±10%.

4. Analysis of the results

The data obtained make it possible to perform a comparative analysis of the parametric superluminescence and singly resonant OPO regimes.

The dependences in Figs 2 and 6 show that the presence of a dense cavity at the signal wavelength in comparison with the superluminescence regime lowers the generation threshold by a factor of ~1.7 (from 100 to 60 mW) and increases the average output power at the idler wavelength from ~30 to ~60 mW. This behaviour is related to the energy accumulation in the cavity at the signal wavelength under synchronous pumping. The increase in the number of signal-wave photons leads to a decrease in the threshold pump power and an increase in the idler wave power, because generation of the difference frequency of these (signal and pump) waves occurs in the cavity:

$$\hbar\omega_i = \hbar\omega_p - \hbar\omega_s, \qquad k_p - k_s = k_i + 2\pi/\Lambda \tag{6}$$

The lower (in comparison with the results of [6]) conversion efficiency in the superluminescence regime is explained by the lower quality of the crystal in use. It was found from Fig. 2 that the ratio of the number of signal photons to the number of idler photons, averaged over the entire measurement range, amounts to ~1.3; this circumstance indicates the presence of absorption in the crystal (~20%) in the vicinity of $\lambda = 3.8$ μm, as was noted in [6].

The generation threshold in the superluminescence regime is ~200 MW cm^{-2}, which is approximately coincides with the calculated value: ~160 MW cm^{-2} [10]. Under synchronous pumping of a singly resonant OPO, the measured threshold (~120 MW cm^{-2}) is almost an order of magnitude larger than that calculated using the formulae from [11, 12]. Apparently, this is related to the specific features of exact experimental determination of the generation threshold.

The pump depletion coefficient in the singly resonant OPO regime turned out to be ~55%, whereas in the superluminescence regime it was about 45% for one pass and 50% for two passes. Hence, there is no point in applying longer nonlinear crystals. The reason is that the gain is saturated for one pass when the generation threshold is exceeded by a factor of 5 or more, which is in good agreement with the results of the theoretical analysis performed in [14]. Since the maximum excess of the pump power above the threshold was 4 and 6.5 times in the superluminescence and singly resonant OPO regimes, the pump depletion coefficients, according to [14], should be 65% and 70%, respectively. The difference in the results is due to the fact that pump radiation used in the theoretical model [14] was single-mode, whereas in this study we applied a laser operating in the multimode regime, which is characterised by a lower conversion efficiency [15].

5. Conclusions

We investigated a cavity-free OPO in the superluminescence regime and a singly resonant OPO synchronously pumped by a Q-switched mode-locked Nd:YAG laser by the spherical mirror–acousto-optic modulator (SMAOM) method [9, 16]. It was shown that the presence of a cavity leads to an increase in the conversion efficiency into the idler wave by a factor of about 2 and a decrease in the generation threshold by a factor of no less than 1.7 in comparison with the superluminescence regime.

In the superluminescence regime, the output radiation spectrum contains a high-power signal wave, and the total conversion efficiency with respect to the absorbed power is fairly high (60%–80%). This efficiency can be significantly increased by generating high-power tunable radiation in the red spectral region via summation of the signal and pump waves. To this end, it is sufficient to place a PPLN crystal with a period Λ behind the PPLN crystal under study in order to generate the sum frequency. As was noted above, this radiation with a tunable generation line will have the same divergence as the IR parametric superluminescence. An evident advantage of the superluminescent OPO regime is the absence of cavity and, therefore, necessity of its matching with the pump laser cavity.

References

1. Graf T., McConnell G., Ferguson A.I., et al. *Appl. Opt*., **38**, 3324 (1999).
2. Donin V.I., Yakovin D.V., Yakovin M.D. *Quantum Electron*., **46**, 601 (2016) [*Kvantovaya Elektron*., **46**, 601 (2016)].
3. Zayhowski J.J. *Opt. Lett*., **22**, 169 (1997).
4. Sudmeyer T., Aus der Au J., Paschotta R., et al. *J. Phys. D: Appl. Phys*., **34**, 2433 (2001).
5. Kir'yanov A.V., Klimentov S.M., Powers P.E., et al. *Laser Phys. Lett*., **5**, 281 (2008).
6. Donin V.I., Yakovin D.V., Yakovin M.D., Gribanov A.V. *Laser Phys. Lett*., **15**, 035005 (2018).
7. Zhang X., Wang Y., Ju Y., et al. *Chin. Opt. Lett*., **6**, 204 (2008).
8. Donin V.I., Yakovin D.V., Gribanov A.V. *Quantum Electron*., **45**, 1117 (2015) [*Kvantovaya Elektron*., **45**, 1117 (2015)].
9. Donin V.I., Yakovin D.V., Gribanov A.V., Yakovin M.D. *J. Opt. Technol*., **85** (4), 193 (2018) [*Opt. Zh*., **85** (4), 8 (2018)].
10. Agnesi A., Piccinini E., Reali G.C., Solcia C. *Opt. Lett*., **22**, 1415 (1997).
11. Guha S., Wu F.-J., Falk J. *IEEE J. Quantum. Electron*., **18**, 907 (1982).
12. Cheung E.C., Liu J.M. *J. Opt. Soc. Am. B*, **7**, 1385 (1990).
13. Gribanov A.V., Donin V.I., Yakovin D.V. *Quantum Electron*., **48**, 699 (2018) [*Kvantovaya Elektron*., **48**, 699 (2018)].
14. Bjorkholm J.E. *IEEE J. Quantum Electron*., **7**, 109 (1971).
15. Marshall L.R., Kaz A., Aytur O. *IEEE J. Quantum Electron*., **32**, 177 (1996).
16. Donin V.I., Yakovin D.V., Gribanov A.V. *Quantum Electron*., **42**, 107 (2012) [*Kvantovaya Elektron*., **42**, 107 (2012)].